A CNN-LSTM Phase Compensation Method for Unidirectional Two-way Radio Frequency Transmission System

Jiahui Cheng, Zhengkang Wang, Yaojun Qiao, Hao Gao, Chenxia Liu, *Member, IEEE*, Zhuoze Zhao, Jie Zhang, *Student Member, IEEE*, Baodong Zhao, Bin Luo, and Song Yu

***Abstract*—A convolutional neural network combined with long short-term memory (CNN-LSTM) phase compensation method (PCM) is proposed and demonstrated, where CNN is employed to extract spatial features, and LSTM is used to capture temporal features and realize the long-term predictions of residual phase fluctuations. This is the first-time machine learning (ML) has been used to mitigate the effects of optical path asymmetry caused by temperature variations on radio frequency (RF) transmission systems. The performance is verified by experiments on a unidirectional two-way RF transmission system, in which both the two 259-km-long separate fibers are coupled into one optical cable. The results demonstrate the CNN-LSTM model presents better prediction performance than the other eight previously proposed ML models. When the prediction duration is 40,000 s and the ambient temperature variation range is 14.38 °C, the coefficient of determination (R Squared, R2) between the predicted value and the actual value is higher than 0.99. In addition, compared to the phase locked loop (PLL) PCM, the proposed CNN-LSTM PCM can reduce the root-mean-square (RMS) phase jitter of the received signal from 219 ps to 19.72 ps, and improve the frequency stability of the system at 10,000 s by 84.5%. Overall, the proposed CNN-LSTM PCM can effectively compensate for residual phase fluctuations generated by the optical path asymmetry, providing a potential option for achieving stable RF transmission in telecommunication networks.**

***Index Terms*—Convolutional neural network, frequency transmission, long short-term memory network, unidirectional two-way, frequency stability.**

Manuscript received 9 November 2023; revised 19 April 2024; accepted 29 April 2024. Date of publication 1 May 2024; date of current version 13 May 2024. This work was supported by the Beijing University of Posts and Telecommunications (BUPT) Excellent Ph.D. Students Foundation under Grant CX2022112. *(Corresponding author: Bin Luo.)*

Jiahui Cheng, Yaojun Qiao, Hao Gao, Zhuoze Zhao, Jie Zhang, Baodong Zhao, Bin Luo, and Song Yu are with the State Key Laboratory of Information Photonics and Optical Communications, Beijing University of Posts and Telecommunications, Beijing 100876, China (e-mail: cheng_jh@bupt.edu.cn; qiao@bupt.edu.cn; hao@bupt.edu.cn; zhaozhuoze@bupt.edu.cn; zhang-jie@bupt.edu.cn; zhaobaodong@bupt.edu.cn; luobin@bupt.edu.cn; yusong@bupt.edu.cn).

Zhengkang Wang is with the Laboratory of Space-Ground Interconnection and Convergence, School of Information and Communication Engineering, Beijing University of Posts and Telecommunications, Beijing 100876, China (e-mail: 864125399@qq.com).

Chenxia Liu is with the Department of Electronic and Communication Engineering, North China Electric Power University, Baoding 071066, China (e-mail: liuchenxia2413@ncepu.edu.cn).

Digital Object Identifier 10.1109/JPHOT.2024.3395834

I. Introduction

A LARGE number of advanced scientific and industrial fields rely on high-precision frequency transmission, such as atomic clock comparison, navigation and positioning, and very long baseline interferometry (VLBI) [1], [2], [3]. Nowadays, standard telecommunication networks present excellent characteristics and have been applied all over the world. To further expand the application range of radio frequency (RF) transmission, the stable RF transmission in telecommunication networks has attracted extensive attention of researchers [4].

Theoretical research shows that optical fiber links are sensitive to temperature variations, mechanical perturbations, and laser wavelength drifts, which cause the phase fluctuations of the transmitted signal. Therefore, it is necessary to compensate for the phase fluctuations to achieve stable RF transmission in optical fiber link. Currently, high-precision frequency synchronization schemes generally require bidirectional transmission of signals in the same fiber, where the phase fluctuations of the two propagation directions are highly correlated, therefore the phase fluctuations of the uplink can almost perfectly compensate for the phase fluctuations in the downlink [5], [6]. However, the above scheme is in conflict with the existing telecommunication networks, which are equipped with unidirectional amplifiers, and the optical signals can only be transmitted in one direction along the link. In a standard telecommunication network, RF transmission can be accomplished using two methods. One method is to modify the unidirectional link into a bidirectional link for signal transmission [7], [8], [9], which is more stable, but costly and complicated to operate. An alternative method involves using two unidirectional optical fiber links for round-trip transmission of RF signals, known as the unidirectional two-way RF transmission system [10], [11]. The unidirectional two-way RF transmission system does not require any modifications to existing telecommunications networks. However, the stability of the system is affected by the residual phase fluctuations generated by the asymmetry between the uplink and the downlink caused by temperature variations [12]. When the system is used for a long-term working environment, the accumulated residual phase fluctuations can deteriorate the received signal's long-term frequency stability. Therefore, the study of how to compensate for the residual phase fluctuations and improve the stability of

the unidirectional two-way RF transmission system effectively is of great significance.

Recently, research on machine learning (ML) has ignited massive applications both in industry and academia [13], [14], [15]. In the field of optical fiber communication systems, ML has also been investigated to solve important problems, such as resisting noise interference [16] and predicting nonlinear time series [17]. The convolutional neural network (CNN) [18] and the long short-term memory (LSTM) [19] are two effective network architectures in ML. CNN is a type of feedforward neural network, which can extract spatial features from data effectively. The local perception and weight sharing characteristic of CNN can greatly reduce the number of parameters, and improve the model learning efficiency [20], [21]. LSTM networks are extensions of recurrent neural networks (RNNs), not only able to learn temporal correlations in series prediction problems, but also able to memorize information for a long time. In recent studies, the LSTM has achieved good results in nonlinear time series prediction, such as voltage prediction [22], pressure prediction [23], and GNSS time series prediction [24]. The residual phase fluctuations of the system cannot be obtained in advance, but its changing trend is related to temperature variations and the uplink phase fluctuations, all three of which are typical nonlinear time series. Therefore, the CNN-LSTM model can be used to capture the intrinsic connection between the three. In this way, we can predict the residual phase fluctuations of the system based on the temperature variations and uplink phase fluctuations during the system operation, and compensate for it to improve the stability of the unidirectional two-way RF transmission system.

In this paper, a CNN-LSTM phase compensation method (PCM) is proposed to predict and compensate for the residual phase fluctuations generated by the asymmetry between the uplink and downlink caused by temperature variations, and to improve the long-term frequency stability of the unidirectional two-way RF transmission system. The CNN is employed to extract spatial features, and the LSTM is used to capture temporal features and predict residual phase fluctuations for a long-term. By experimenting on 2.4 GHz unidirectional two-way radio frequency (RF) transmission system with a transmission distance of 259 km, the results demonstrate that: the CNN-LSTM model can effectively capture the nonlinear features of the residual phase fluctuations, and has better prediction performance than the other eight previously proposed ML models. When the prediction duration is 40000 s and the ambient temperature variation range is 14.38 °C, the coefficient of determination (R Squared, R^2) between the predicted and the actual values is 0.9919, which is 79.49%, 41.36%, 12.26%, 7.84%, 3.97%, 2.70%, 2.33%, and 0.38% better than Random Forest Regression (RFR), Support Vector Regression (SVR), bidirectional long short-term memory (Bi-LSTM), Back Propagation Neural Network (BPNN), RNN, Gated Recurrent Units (GRU), LSTM, and CNN-GRU models, respectively. Moreover, compared to the phase locked loop (PLL) PCM, the proposed CNN-LSTM PCM can reduce the root-mean-square (RMS) phase jitter of the received signal from 219 ps to 19.72 ps during a measurement time of 40000 s, and improve the frequency stability of the system at 10000 s by 84.5%.

II. Principle of the Proposed Method

A. Principle of the CNN-LSTM Model

The main structures of the CNN-LSTM model are the CNN and the LSTM. The CNN is employed to extract spatial features from input data, while the LSTM is used to capture temporal features and make long-term predictions. Fig. 1 shows the architecture diagram of the CNN-LSTM model, which comprises input layer, convolution layer, pooling layer, LSTM layer, and output layer. In this study, the input of the CNN-LSTM model is ambient temperature and uplink's phase fluctuations. The output is system's residual phase fluctuations.

CNN is the base layer of CNN-LSTM model, which mainly consists of convolutional layer and pooling layer. The convolutional layer extracts spatial features of multivariate time series using multiple convolutional filters. If $x_i = \{x_1, x_2, \cdots, x_n\}$ is the input vector, the output from the convolutional layer can be represented as

$$y_{ij} = \sigma\left(b_j + \sum_{m=1}^{M} w_{m,j} x_{i+m-1,j}\right). \tag{1}$$

Where y_{ij} is the output from the convolutional layer, σ represents the activation function, $m$is the index value, w is the weight of the filter, $x_{i,j}$ is the input layer and b_j is the bias for the j^{th} feature. The pooling layer is added after the convolution layer to reduce the feature dimension of the network, and also has the effect of adjusting the overfitting. (2) represents the operation of the max-pooling layer. S is the stride that decide how far to move the area of input data, and R is the pooling size of less than the size of the input$y$.

$$p_{ij} = \max_{\substack{i \times S + r, j \\ r \in R}}^{l-1}. \tag{2}$$

LSTM, which is a lower layer of CNN-LSTM. The structure of an LSTM unit is configured by a cell and three gates, that is: the forget gate, input gate and output gate. The forget gatef_t responsible for determining the information that should be removed from the cell state, it can be expressed as

$$f_t = \sigma(w_f \cdot [h_{t-1}, p_t] + b_f), \tag{3}$$

where $\sigma(\cdot)$ is the sigmoid function, h_{t-1} is the output of the LSTM unit at timestep $(t-1)$, p_t is the output of the pooling layer, $[h_{t-1}, p_t]$ represents a vector concatenated by h_{t-1} andp_t. w_f and b_f are the weight matrix and bias vector of the forget gate, respectively. The input gate can determine which information to put into the current cell state, the sigmoid function determines the value i_t to be updated, and the tanh function is used to create a new candidate vector $\tilde{c}_t$ .The calculation process of the input gate is

$$i_t = \sigma(w_i \cdot [h_{t-1}, p_t] + b_i), \tag{4}$$

$$\tilde{c}_t = \tanh(w_c \cdot [h_{t-1}, p_t] + b_c), \tag{5}$$

where $tanh(\cdot)$ is the hyperbolic tangent function, w_i, b_i and w_c, b_c are the weight matrix and bias vector of the input gate, and the state update vector, respectively. The output gate receives new information by multiplying the output intermediate cell state $\tilde{c}_t$

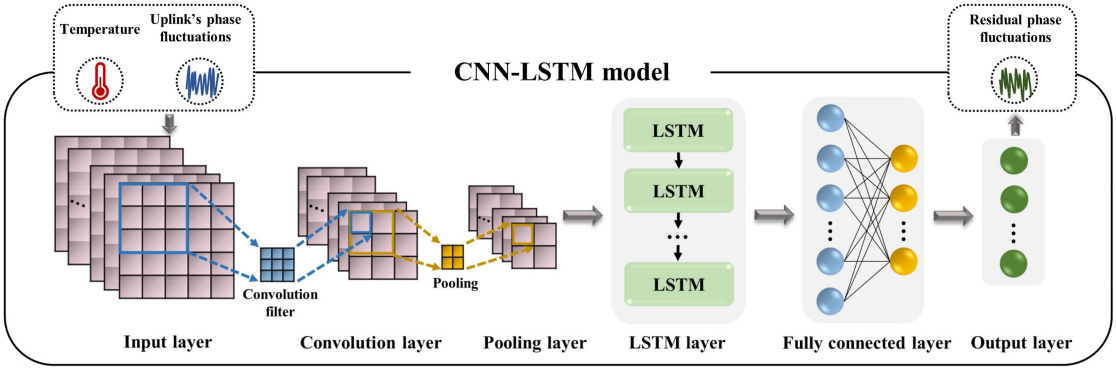

Fig. 1. The architecture diagram of the CNN-LSTM model.

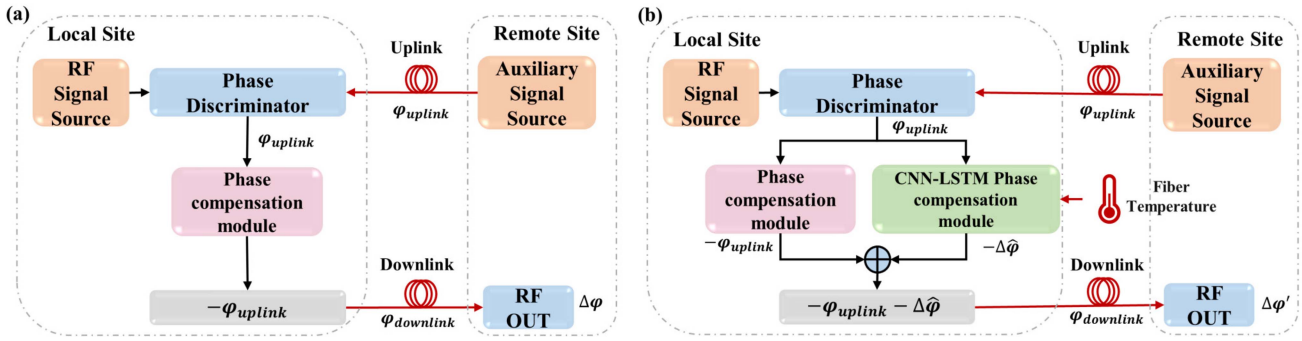

Fig. 2. The schematic diagram of the unidirectional two-way RF transmission system: (a) without CNN-LSTM phase compensation module, (b) with CNN-LSTM Phase compensation module.

by the result of the input gate i_t. It also updates the cell state by discarding data by multiplying the past state c_{t-1} by the result of the forget gate f_t. The output h_t of LSTM is calculated using the finally updated cell state and the output gate o_t. These calculations can be expressed as

$$c_t = f_t \circ c_{t-1} + i_t \circ \tilde{c}_t, \tag{6}$$

$$o_t = \sigma(w_o \cdot [h_{t-1}, p_t] + b_o), \tag{7}$$

$$h_t = o_t \circ \tanh(c_t). \tag{8}$$

The last layer of CNN-LSTM is the fully connected layer. The output of the LSTM unit is flattened to a feature vector$h^l = \{h_1, h_2, \cdots h_l\}$, l is the number of units in LSTM. The output of the LSTM is used as the input to the fully connected layer. (9) shows the equation used in this layer. σ is a non-linear activation function, w is the weight of the i^{th}node for layer $l-1$ and the j^{th} node for layer l, and b_i^{l-1} represents a bias vector of the fully connected layer.

$$d_i^l = \sum_j w_{ji}^{l-1} \left(\sigma\left(h_i^{l-1}\right) + b_i^{l-1}\right). \tag{9}$$

B. Principle of the CNN-LSTM PCM

Fig. 2 shows the schematic diagram of the unidirectional two-way RF transmission system without/with the CNN-LSTM phase compensation module. The reference signal generated by the remote auxiliary signal source is transmitted to the local site (LS) along the uplink. This signal is discriminated with the reference signal to obtain the phase fluctuations of the uplink φ_{uplink}. In the classical PCM, as shown in Fig. 2(a), φ_{uplink} is used as the pre-compensation phase to compensate the phase fluctuations of the downlink $\varphi_{downlink}$ when the signal is transmitted to the remote site (RS) along the downlink. The residual phase fluctuations of the system after compensation by the classical PCM can be expressed as

$$\Delta\varphi = \varphi_{downlink} - \varphi_{uplink}. \tag{10}$$

In the CNN-LSTM PCM, as shown in Fig. 2(b). The CNN-LSTM network can obtain the predicted value of the residual phase fluctuations $\Delta\widehat{\varphi}$ based on the uplink's phase fluctuations and ambient temperature. $\Delta\widehat{\varphi}$ will compensate the phase fluctuations of the downlink together with the pre-compensation phase$-\varphi_{uplink}$ provided by the classical PCM. The residual phase fluctuations of the system after compensation by the CNN-LSTM PCM can be expressed as

$$\Delta\varphi' = \varphi_{downlink} - \varphi_{uplink} - \Delta\widehat{\varphi} = \Delta\varphi - \Delta\widehat{\varphi}. \tag{11}$$

III. Experimental Setup and Model Construction

A. Experimental Setup

In order to analyze the performance of the proposed method, we set up a 2.4 GHz unidirectional two-way RF transmission

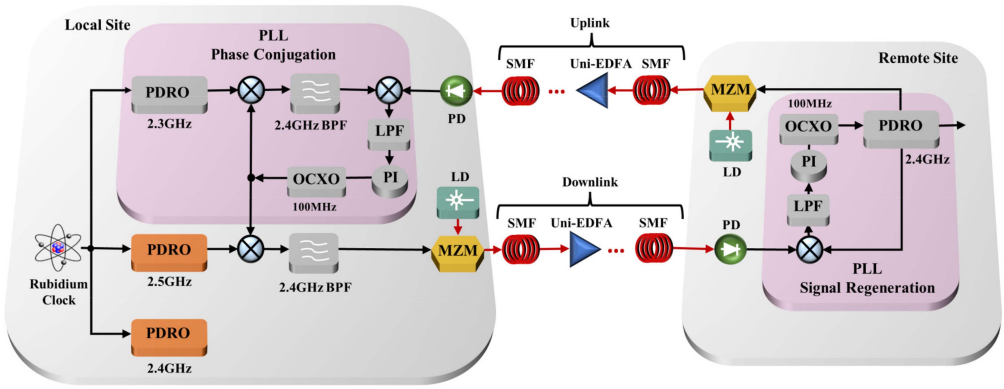

Fig. 3. The schematic diagram of the unidirectional two-way RF transmission system based on PLL PCM. PLL: phase locked loop. PDRO: phase-locked dielectric resonant oscillator. BPF: band pass filter. LPF: low pass filter. PI: proportional integral controller. OCXO: oven-controlled crystal oscillator. PD: photo-detector. LD: laser diode. MZM: Mach–Zehnder modulator. SMF: single-mode fiber. Uni-EDFA: unidirectional-erbium doped fiber amplifier.

system based on PLL PCM. Two 259-km-long fibers are coupled into one optical cable, and four unidirectional-erbium doped fiber amplifiers (Uni-EDFAs) are installed on both the uplink and the downlink. The proper dispersion compensation fiber (DCF) is contained to reduce the asymmetry of time delay between the two directions due to group velocity dispersion. The schematic diagram of the unidirectional two-way RF transmission system based on PLL PCM is shown in Fig. 3. The system synchronizes the 2.4 GHz RF signal at the RS with the 2.4 GHz RF signal at the LS, which is locked to a rubidium clock (Quartzlock, A1000). There are mainly three steps involved in phase fluctuations cancellation. At first, the 2.4 GHz RF signal at RS is intensity modulated on the optical carrier and transmitted to the LS via uplink. The photo-detector (PD) at the LS can detect the 2.4 GHz RF signal carrying the uplink's phase fluctuations φ_{uplink}. φ_{uplink} can be measured by a high precision digital multimeter (Keysight 34465A). Then, the PLL and the auxiliary RF signal (2.5 GHz) complete the phase conjugation at the LS [25]. Finally, the pre-compensated phase is transmitted to the RS via downlink, which is used to compensate for the phase fluctuations of the downlink $\varphi_{downlink}$. The PLL at the RS acts as signal regenerator, it improves the signal-to-noise ratio (SNR) of the transmitted signal. The phase fluctuations $\Delta\varphi$ of the 2.4 GHz RF signal at the RS is the residual phase fluctuations introduced by incomplete compensation. The temperature of the optical cable can be measured by the temperature sensor.

In practical applications, optical fiber links are generally distributed over a large area, at which time we will capture temperature information from multiple nodes for model training. In addition, the model input is not only the temperature but also the uplink's phase fluctuations, mainly caused by the temperature variations, so even when temperature information is difficult to collect, the model can capture the temperature information from the uplink phase fluctuations, which is also why we choose multiple input variables for model training.

B. Construction of CNN-LSTM Model

CNN-LSTM model is constructed using 400000 sets of sample data from a unidirectional two-way RF transmission system based on PLL PCM (Fig. 3), with a sampling interval of 1 s and an average daily temperature variation range of 15.22 °C. Each set of sample data contains three features, including uplink's phase fluctuations, ambient temperature around the fiber, and system's residual phase fluctuations. To reduce the pressure on the model for long-term prediction, we down-sampled 400000 sets of sample data at equal intervals to 800 sets (sampling interval of 500). These data are divided into three groups: the training set (80%), the validation set (10%) and the testing set (10%). The validation data set is used to ensure that the network will perform well on new data and avoid overfitting. We build the CNN-LSTM network based on Keras package using TensorFlow as the backend. The parameter settings of the CNN-LSTM used in this experiment are shown in Table I.

TABLE I
THE PARAMETER SETTINGS OF THE CNN-LSTM MODEL

Parameters	Value
Convolution layer filters	64
Convolution layer kernel size	3
Convolution layer activation function	Relu
Pooling layer pool size	2
Pooling layer activation function	Relu
Number of hidden units in LSTM layer	32
LSTM layer activation function	Relu
Time step	60
Batch size	32
Learning rate	0.001
Optimizer	Adam
Loss function	Mean absolute error
Epochs	100

IV. Results and Discussion

A. The Prediction Performance of CNN-LSTM Model

The performance of the constructed CNN-LSTM model is verified on a newly collected dataset. The model is used to predict residual phase fluctuations in the future 80-time steps.

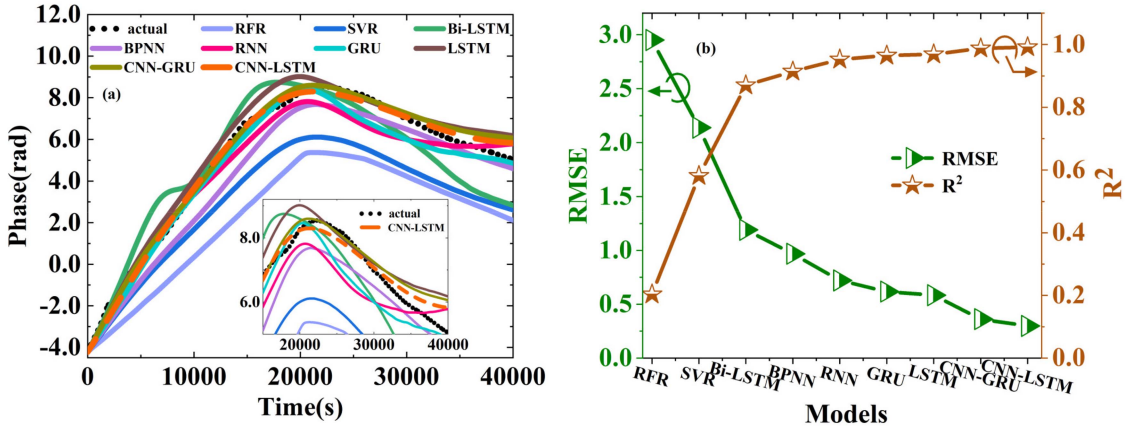

Fig. 4. (a) The prediction results of different models. (b) The RMSE and R^2 of different models.

It is necessary to interpolate the predicted data to restore the original data. A second-order curve interpolation method is used to restore 80 predicted values to 40000 by inserting 500 points between two-time steps. In order to demonstrate the effectiveness of the CNN-LSTM model, we constructed eight other ML models using the same dataset: RFR, SVR, Bi-LSTM, BPNN, RNN, GRU, LSTM and CNN-GRU. Fig. 4(a) shows the prediction results of different models for a time period of 40000 s with an ambient temperature variation range of 14.38 °C. In the nine models, CNN-LSTM is the model with the highest correlation between the predicted value and the actual value. The predicted curve of phase fluctuations (orange dashed line) is almost coincident with the actual curve (black dashed line). Followed by CNN-GRU, LSTM, GRU, RNN, BPNN, Bi-LSTM, SVR, and RFR.

To evaluate the prediction performance of CNN-LSTM, mean absolute error (MAE), root mean squared error (RMSE) and R^2 are used as evaluation criteria of different methods. The calculation formulas of the three evaluation criteria can be expressed as follows:

$$MAE = \frac{1}{n}\sum_{i=1}^{n}\left|\Delta\varphi_i - \Delta\widehat{\varphi}_i\right| \tag{12}$$

$$RMSE = \frac{1}{n}\sqrt{\sum_{i=1}^{n}\left(\Delta\varphi_i - \Delta\widehat{\varphi}_i\right)^2} \tag{13}$$

$$R^2 = 1 - \frac{\sum_{i=1}^{n}\left(\Delta\varphi_i - \Delta\widehat{\varphi}_i\right)^2}{\sum_{i=1}^{n}\left(\Delta\varphi_i - \Delta\bar{\varphi}_i\right)^2} \tag{14}$$

Where $\Delta\varphi_i$, $\Delta\widehat{\varphi}_i$ and $\Delta\bar{\varphi}_i$ denote the actual, predicted and average value of residual phase fluctuations respectively, and n is the number of test samples.

Fig. 4(b) shows the RMSE and R^2 between the predicted value and actual value of different models, and the RMSE and R^2 are represented by the green and brown curves, respectively. Columns 2, 3, and 4 of Table II present the calculated results of three evaluation criteria. Model predictions are more accurate when MAE, RMSE are close to 0, and R^2 is close to 1. The MAE and RMSE of the CNN-LSTM model are 0.2442 and 0.2981, respectively, which are the smallest of the nine models. The R^2 of the CNN-LSTM model is 0.9919, which is the largest of the nine models. It is 79.49%, 41.36%, 12.26%, 7.84%, 3.97%, 2.70%, 2.33%, and 0.38% higher than RFR, SVR, Bi-LSTM, BPNN, RNN, GRU, LSTM, and CNN-GRU models, respectively. This indicates that the CNN-LSTM model has better prediction performance than the other eight previously proposed ML models. Compared to other ML models, the CNN-LSTM model not only utilizes CNN's powerful weight sharing ability to extract the features of the input data effectively, but also takes full advantage of the three gates (the forget gate, input gate and output gate) of LSTM that can selectively memorize information. The coordinated cooperation of the three gates not only overcomes the gradient vanishing problem existing in RNN, but also memorizes the temporal correlation of the phase fluctuations data for a long time. Therefore, the CNN-LSTM model captures the nonlinear features of the residual phase fluctuations effectively performs better in long time prediction.

TABLE II
RMSE, MAE, R^2 AND TIME COMPLEXITY OF DIFFERENT PREDICTION MODELS

Models	RMSE	MAE	R^2	Time Complexity
RFR	2.9503	2.8577	0.2035	$O(N * dMlog(N))$
SVR	2.1383	2.0510	0.5816	$O(N^3)$
Bi-LSTM	1.1906	1.005	0.8703	$O(2 * N * (4h^2 + 4hd))$
BPNN	0.9689	0.8686	0.9141	$O(N * dm)$
RNN	0.7206	0.5954	0.9525	$O(N * (h^2 + hd)$
GRU	0.6177	0.5093	0.9651	$O(N * (3h^2 + 3hd + 3h))$
LSTM	0.5839	0.4876	0.9688	$O(N * (4h^2 + 4hd))$
CNN-GRU	0.3613	0.2704	0.9881	$O(N * (kd^2 + 3h^2 + 3hd + 3h))$
CNN-LSTM	**0.2981**	**0.2442**	**0.9919**	$\boldsymbol{O(N * (kd^2 + 4h^2 + 4hd))}$

M: Number of trees; N: Training samples; d: Size of input data; h: Number of hidden units in LSTM layer; m: Neurons in hidden layer; k: Convolution layer kernel size.

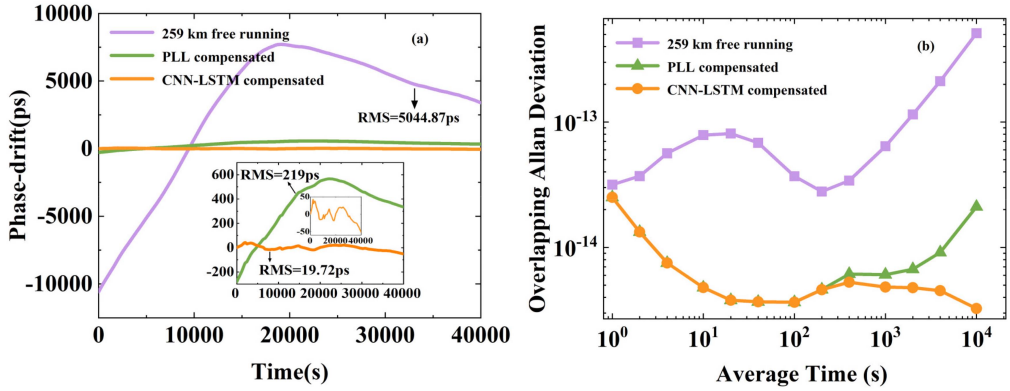

Fig. 5. (a) The residual phase jitter and (b) the OADEV of the uncompensated system, PLL phase compensation system, and CNN-LSTM phase compensation system.

In order to fully analyze the model performance, we compare the time complexity of the nine ML models in the last column of Table II. The complexity of the nine models can be categorized into the following four gradients:

1) Lowest Complexity: Typically, RFR and SVR have lower complexity for smaller datasets, but SVR's complexity can grow significantly with the number of samples.

2) Medium Complexity: BPNN and RNN fall into this category, depending on their size and depth.

3) Higher Complexity: LSTM, GRU, and Bi-LSTM have higher computational requirements due to their recurrent nature and the complexity of their gating mechanisms.

4) Highest Complexity: CNN-GRU and CNN-LSTM are the most computationally intensive due to combining convolutional layers with recurrent layers, significantly increasing their parameter count and computational steps.

Among the nine ML models mentioned above, the CNN-LSTM we utilized exhibits the highest complexity, and its outstanding prediction performance relies on complex computational processes. However, this does not affect the performance of the RF transmission system. Because the CNN-LSTM phase compensation module is used to further compensate for the residual phase fluctuations generated by optical path asymmetry caused by temperature variations after PLL compensation. Temperature variation is a slow process, so the CNN-LSTM compensation module does not need to compensate all the time. During the entire compensation process, the PLL compensates the main phase fluctuations of the system in real time, and the CNN-LSTM module compensates for the residual phase fluctuations every 500 s. Therefore, the time complexity of the CNN-LSTM module does not affect the performance of the RF system.

B. The Performance of CNN-LSTM Compensation System

We compare the performance of the uncompensated system (purple curve), the PLL compensated system (green curve), and the CNN-LSTM compensated system (orange curve) in Fig. 5. Fig. 5(a) shows the residual phase fluctuations of the three systems in the form of phase jitter. During a measurement time of 40000 s, with an ambient temperature variation range of 14.38 °C, the asymmetry between the uplink and downlink caused by temperature variations has a significant impact on the unidirectional two-way RF transmission system. The uncompensated system exhibits an RMS phase jitter as high as 5044.87 ps. Following compensation using a PLL, the RMS phase jitter of the system reduces to 219 ps, while compensation using CNN-LSTM further reduces it to 19.72 ps. Hence, CNN-LSTM PCM can efficiently compensate for residual phase fluctuations in the system based on PLL PCM.

Overlapping Allan Deviation (OADEV) is a key index to evaluate the frequency stability of RF transmission systems. A smaller OADEV results in a more stable system. In order to further analyze the compensation performance of the three systems, we show the OADEV curves of all three systems in Fig. 5(b). The OADEV curve for the uncompensated system has a general upward trend and warps severely after 200 s, with an OADEV of 5.11×10^{-13} at 10000 s. In comparison with the uncompensated system, the PLL compensated system's OADEV curve de significantly lower, but the curve is still warping after 200 s. This indicates that although the PLL system can compensate most of the phase fluctuations in the unidirectional two-way RF transmission system, the long-term stability of the system is still impacted by uncompensated phase fluctuations, primarily generated by asymmetry between the uplink and downlink caused by temperature variations. However, the OADEV curve of the CNN-LSTM compensated system still shows a decreasing trend after 200 s. This indicates CNN-LSTM can further compensate for the residual phase fluctuations. The OADEV of the PLL phase compensation system and the CNN-LSTM compensation system at 10000 s is 2.11 × 10-14 and 3.26 × 10-15, respectively. It is evident that the proposed CNN-LSTM PCM can improve the frequency stability of the system at 10000 s by 84.5 compared to the PLL PCM.

C. Discussion

Compared with the PLL PCM, CNN-LSTM PCM can further compensate for the residual phase fluctuations generated by the asymmetry between the uplink and downlink caused by temperature variations, thereby improving the long-term frequency stability of the unidirectional two-way RF transmission system.

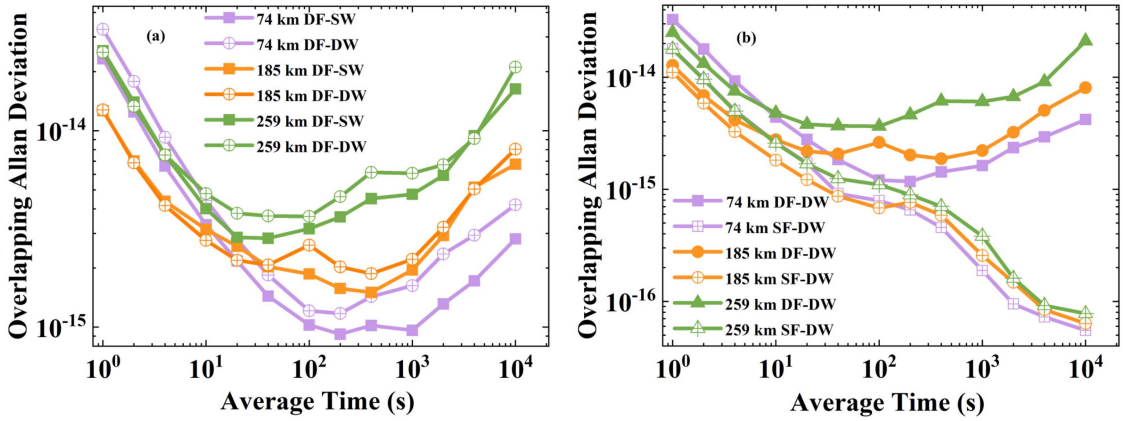

Fig. 6. (a) The OADV of DF-SW and DF-DW system. (b) The OADV of SF-DW and DF-DW system. In DF-SW system, the optical signal wavelengths of both the LS and the RS are 1553.33 nm (30#), and in DF-DW system, the optical signal wavelengths of the LS and RS are 1553.33 nm (30#) and 1550.12 nm (34#), respectively.

However, the specific source of the asymmetry between the uplink and downlink requires to be investigated and analyzed. There are three factors that limit the long-term frequency stability of the system: the wavelength difference between the LS and the RS, the number of amplifiers, and the length asymmetry between the uplink and downlink. In order to determine the primary restriction, we analyze the effects of the above three factors on the frequency stability of the unidirectional two-way RF transmission system based on PLL PCM (as shown in Fig. 3) under different experimental conditions.

When the wavelengths of optical signals used between LS and RS are different, the time delay difference introduced by temperature-induced variation of group velocity dispersion (TIVGVD) cannot be alleviated by dispersion compensation technology, resulting in asymmetry in the round-trip transmission of signals. We measure the frequency stability of the unidirectional two-way RF transmission system with the same wavelength (DF-SW) and different wavelengths (DF-DW) over distances of 74 km, 185 km, and 259 km, respectively, the results are shown in Fig. 6(a). Under the same transmission distance, the long-term stability of the DF-SW system is slightly better than that of the DF-DW system, which is most noticeable in the system with a transmission distance of 74 km. However, as transmission distance increases, whether it is a DF-SW or DF-DW system, its long-term stability will decrease significantly. Long-term stability of the system is much more significantly influenced by transmission distance than wavelength asymmetry. Therefore, we can conclude that the wavelength difference between the LS and the RS is not the primary restriction for the long-term stability of the unidirectional two-way RF transmission system.

The extension of transmission distance implies an increase in the number of amplifiers and an increase in the length asymmetry between the uplink and the downlink. We measure the frequency stability of the single-fiber bi-directional different wavelength (SF-DW) RF transmission system over distances of 74 km, 185 km, and 259 km, and compare the results with those of the DF-DW system. The experimental setup of the SF-DW system is the same as that of the DF-DW system. The number of amplifiers in 74 km, 185 km and 259 km optical fiber links is 1×2, 3×2 and 5×2 respectively. In Fig. 6(b), the lower three curves are the experimental results of SF-DW system, and the upper three curves are the experimental results of DF-DW system, where the purple, orange and green colors represent the transmission distances of 74 km, 185 km and 259 km, respectively. when the transmission distance is extended, the long-term stability of the SF-DW system deteriorates only slightly, while the long-term stability of the DF-DW system deteriorates significantly. This indicates that the number of amplifiers is not the primary restriction for the long-term stability of the system. When the transmission distance is 259 km, the OADEV of the DF-DW system at 10000 s is 2.11×10^{-14}, whereas the OADEV of the SF-DW system is 1.17×10^{-16}. The only difference between the two systems is that the DF-DW system uses two optical fibers for round-trip transmission of RF signals. Therefore, we can conclude that the length asymmetry between the uplink and downlink is the primary restriction for the long-term stability of the unidirectional two-way RF transmission system, and the longer the transmission distance, the greater the length asymmetry between the uplink and downlink.

V. Conclusion

In this paper, a CNN-LSTM PCM has been proposed and demonstrated, which can predict and compensate for the residual phase fluctuations generated by the asymmetry between the uplink and the downlink caused by temperature variations, and improve the long-term stability of the unidirectional two-way RF transmission system. The performance has been verified by experiments on a 259 km unidirectional two-way RF transmission system. The results demonstrate that the CNN-LSTM model presents better prediction performance than the other eight previously proposed ML models. When the prediction duration is 40000 s and the ambient temperature variation range is 14.38 °C, the R^2 between the predicted value and the actual value is higher than 0.99. Moreover, compared to the PLL PCM, the proposed CNN-LSTM PCM reduces the RMS phase jitter of the received signal from 219 ps to 19.72 ps, and effectively

improves the frequency stability of the system at 10000 s by 84.5%. The proposed CNN-LSTM PCM provides a promising choice for realizing the shared transmission of RF signals and data traffic in telecommunication networks.

REFERENCES

[1] M. Cizek et al., "Coherent fibre link for synchronization of delocalized atomic clocks," *Opt. Exp.*, vol. 30, no. 4, pp. 5450–5464, Feb. 2022, doi: 10.1364/OE.447498.

[2] C. Clivati et al., "Measuring absolute frequencies beyond the GPS limit via long-haul optical frequency dissemination," *Opt. Exp.*, vol. 24, no. 11, pp. 11865–11875, May 2016, doi: 10.1364/OE.24.011865.

[3] Y. He et al., "Long-distance telecom-fiber transfer of a radio-frequency reference for radio astronomy," *Optica*, vol. 5, no. 2, pp. 138–146, Feb. 2018, doi: 10.1364/OPTICA.5.000138.

[4] D. Xu, O. Lopez, A. Amy-Klein, and P.-E. Pottie, "Unidirectional two-way optical frequency comparison and its fundamental limitations," *Opt. Lett.*, vol. 45, no. 21, pp. 6074–6077, Nov. 2020, doi: 10.1364/OL.404866.

[5] Q. Li, L. Hu, J. Zhang, J. Chen, and G. Wu, "Multiple-access relay stations for long-haul fiber-optic radio frequency transfer," *Opt. Exp.*, vol. 30, no. 11, pp. 18402–18414, May 2022, doi: 10.1364/OE.460704.

[6] S. Zhou et al., "Stable RF transmission in dynamic phase correction with Rayleigh backscattering noise suppression," *Opt. Fiber Technol.*, vol. 56, May 2020, Art. no. 102165, doi: 10.1016/j.yofte.2020.102165.

[7] N. Chiodo et al., "Cascaded optical fiber link using the internet network for remote clocks comparison," *Opt. Exp.*, vol. 23, no. 26, pp. 33927–33937, Dec. 2015, doi: 10.1364/OE.23.033927.

[8] O. Lopez et al., "Cascaded multiplexed optical link on a telecommunication network for frequency dissemination," *Opt. Exp.*, vol. 18, no. 16, pp. 16849–16857, Aug. 2010, doi: 10.1364/OE.18.016849.

[9] F. Kéfélian, O. Lopez, H. Jiang, C. Chardonnet, A. Amy-Klein, and G. Santarelli, "High-resolution optical frequency dissemination on a telecommunications network with data traffic," *Opt. Lett.*, vol. 34, no. 10, pp. 1573–1575, May 2009, doi: 10.1364/OL.34.001573.

[10] A. Bercy, F. Stefani, O. Lopez, C. Chardonnet, P.-E. Pottie, and A. Amy-Klein, "Two-way optical frequency comparisons at $5 \times 10 - 21$ relative stability over 100-km telecommunication network fibers," *Phys. Rev. A*, vol. 90, no. 6, Dec. 2014, Art. no. 061802, doi: 10.1103/PhysRevA.90.061802.

[11] K. Turza, P. Krehlik, and Ł. Śliwczyński, "Long haul time and frequency distribution in different DWDM systems," *IEEE Trans. Ultrason., Ferroelect., Freq. Control*, vol. 65, no. 7, pp. 1287–1293, Jul. 2018, doi: 10.1109/TUFFC.2018.2827178.

[12] D. Xu, W.-K. Lee, F. Stefani, O. Lopez, A. Amy-Klein, and P.-E. Pottie, "Studying the fundamental limit of optical fiber links to the 10^{-21} level," *Opt. Exp.*, vol. 26, no. 8, pp. 9515–9527, Apr. 2018, doi: 10.1364/OE.26.009515.

[13] Y. LeCun, Y. Bengio, and G. Hinton, "Deep learning," *Nature*, vol. 521, no. 7553, pp. 436–444, May 2015, doi: 10.1038/nature14539.

[14] G. Chen and C. Jiang, "Transmittance prediction and inverse design of microring resonator channel dropping filters with deep learning," *IEEE Photon. J.*, vol. 14, no. 2, Apr. 2022, Art. no. 8518911, doi: 10.1109/JPHOT.2022.3157776.

[15] J. Xu, Y. Mao, Y. Chen, X. Xu, and Y. Guo, "Machine learning assisted prediction for free-space continuous variable quantum teleportation," *IEEE Photon. J.*, vol. 14, no. 4, Aug. 2022, Art. no. 7639407, doi: 10.1109/JPHOT.2022.3186391.

[16] J. Xue, L. Zhao, T. Wang, L. Zhao, and F. Cui, "A novel compact Fiber optic concentration sensing system based on machine learning demodulation," *IEEE Photon. J.*, vol. 15, no. 4, Aug. 2023, Art. no. 7100906, doi: 10.1109/JPHOT.2023.3290984.

[17] F. N. Khan, Q. Fan, C. Lu, and A. P. T. Lau, "An Optical Communication's perspective on machine learning and its applications," *J. Lightw. Technol.*, vol. 37, no. 2, pp. 493–516, Jan. 2019, doi: 10.1109/JLT.2019.2897313.

[18] Y. Lecun, L. Bottou, Y. Bengio, and P. Haffner, "Gradient-based learning applied to document recognition," in *Proc. IEEE*, 1998, vol. 86, no. 11, pp. 2278–2324, doi: 10.1109/5.726791.

[19] S. Hochreiter and J. Schmidhuber, "Long short-term memory," *Neural Computation*, vol. 9, no. 8, pp. 1735–1780, Nov. 1997, doi: 10.1162/neco.1997.9.8.1735.

[20] O. Kliebisch, H. Uittenbosch, J. Thurn, and P. Mahnke, "Coherent Doppler wind LiDAR with real-time wind processing and low signal-to-noise ratio reconstruction based on a convolutional neural network," *Opt. Exp.*, vol. 30, no. 4, pp. 5540–5552, Feb. 2022, doi: 10.1364/OE.445287.

[21] G. Kaur et al., "Face mask recognition system using CNN model," *Neurosci. Inform.*, vol. 2, no. 3, Sep. 2022, Art. no. 100035, doi: 10.1016/j.neuri.2021.100035.

[22] Y. Chen, "Voltages prediction algorithm based on LSTM recurrent neural network," *Optik*, vol. 220, Oct. 2020, Art. no. 164869, doi: 10.1016/j.ijleo.2020.164869.

[23] Y. Mei, S. Zhang, Z. Cao, T. Xia, X. Yi, and Z. Liu, "Deep learning assisted pressure sensing based on Sagnac interferometry realized by side-hole fiber," *J. Lightw. Technol.*, vol. 41, no. 2, pp. 784–793, Jan. 2023, doi: 10.1109/JLT.2022.3220543.

[24] W. Gao, Z. Li, Q. Chen, W. Jiang, and Y. Feng, "Modelling and prediction of GNSS time series using GBDT, LSTM and SVM machine learning approaches," *J. Geodesy*, vol. 96, no. 10, Oct. 2022, Art. no. 71, doi: 10.1007/s00190-022-01662-5.

[25] C. Liu et al., "Ultrastable long-haul Fiber-optic radio frequency transfer based on dual-PLL," *IEEE Photon. J.*, vol. 13, no. 1, Feb. 2021, Art. no. 7100108, doi: 10.1109/JPHOT.2020.3043263.